

## Engineered method for directional growth of muscle sheets on electrospun fibers

Erfan Soliman<sup>1</sup>, Fabio Bianchi<sup>1</sup>, James N Sleight<sup>2‡</sup>, Julian H George<sup>1</sup>, M Zameel Cader<sup>2</sup>, Zhanfeng Cui<sup>1</sup>, and Hua Ye<sup>1</sup>

1 Institute of Biomedical Engineering, Department of Engineering Sciences, Old Road Campus Research Building, University of Oxford, Oxford OX3 7DQ, UK

2 The Weatherall Institute of Molecular Medicine, University of Oxford, John Radcliffe Hospital/Headley Way, Oxford OX3 9DS, UK

‡ Present address: Sobell Department of Motor Neuroscience and Movement Disorders, Institute of Neurology, University College London, London WC1N 3BG, UK.

Corresponding author:

Prof Hua Ye

hua.ye@eng.ox.ac.uk

+44(0)1865 617689

Institute of Biomedical Engineering, Department of Engineering Science  
Old Road Campus Research Building, University of Oxford  
Headington, Oxford OX3 7DQ UK

This article has been accepted for publication and undergone full peer review but has not been through the copyediting, typesetting, pagination and proofreading process which may lead to differences between this version and the Version of Record. Please cite this article as an 'Accepted Article', doi: 10.1002/jbm.a.36312

## Abstract

Research on the neuromuscular junction (NMJ) and its function and development spans over a century. However, researchers are limited in their ability to conduct experimentation on this highly specialized synapse between motor neurons and muscle fibers, as NMJs are not easily accessible outside the body. The aim of this work is to provide a reliable and reproducible muscle sheet model for *in vitro* NMJ study. A novel culture system was designed by engineering a method for the directional growth of myofiber sheets, using muscle progenitor cells cultured on electrospun fiber networks. Myoblastic C2C12 cells cultured on suspended aligned fibers were found to maintain directionality, with alignment angle standard deviations approximately two-thirds lower on fibers than on regular culture surfaces. Morphological studies found nuclei and cytoskeleton aspect ratios to be elongated by 20% and 150%, respectively. Furthermore, neurons were shown to form innervation patterns parallel to suspended fibers when co-cultured on developed muscle sheets, with alignment angle standard deviations three times lower compared to those on typical surfaces. The effect of agrin on samples was quantified through the slow release of agrin medium, encapsulated in alginate pellets and imbedded within culture chambers. Samples exposed to agrin showed significantly increased percentage of AChR-covered area. The developed model has potential to serve as the basis for synaptogenesis and NMJ studies, providing a novel approach to bio-artificial muscle alignment and setting the groundwork for further investigations in innervation.

**Keywords:** neuromuscular junction, electrospinning, muscle sheet, innervation, aligned scaffold

## Introduction

The vital link between muscle and nerve, where motor neurons release the neurotransmitter acetylcholine to induce muscle contractions, is called the ‘neuromuscular junction’ (NMJ). NMJs are formed during late embryonic development, when axons from motor neurons reach their innervation targets and form synapses [1]. The NMJ appears to be a common target for pathology in a number of neurological conditions, for instance Amyotrophic Lateral Sclerosis (ALS), also known as Motor Neuron Disease (MND) in the UK [2], Charcot-Marie-Tooth disease (CMT) [3], Duchenne Muscular

Dystrophy (DMD), Myotonic Dystrophy (DM), and Spinal Muscular Atrophy (SMA) [4]. Despite their relatively low incidence (e.g. MND has an incidence between 1–3 in 100,000 people per year in the UK [5]), the high treatment cost [6] and extreme debilitation of these diseases have attracted scientific and public attention. A better understanding of the pathogenesis behind such diseases, and an advancement of study models, could help abate the cost of care and increase the effectiveness of treatment [7].

Most neuromuscular conditions involve some malfunctioning of the NMJ, and whilst current *in vitro* models focus on single neuron interactions with cultured myotubes, a scalable, tissue-scale model could offer wider possibilities for drug testing and for disease modeling [8, 9]. For such a model, a reliable approach to muscle sheet formation is required.

In the human body, tissues display varying degrees of alignment, depending on tissue structure, function, and extracellular matrix (ECM) makeup [10]. The ability to manipulate directionality of tissue engineered constructs could thus lead to more realistic tissue models, replicating the complex interactions between cells and ECM occurring *in vivo* [11]. Skeletal muscle exhibits a high degree of alignment; attempts to replicate this have been carried out by culturing on micro patterned substrates [12], electrospun fibers, or mechanical forces [13], as well as in 3D hydrogel cultures [14].

Here, we present a novel technique for *in vitro* culture of myoblast-derived muscle sheets, formed on aligned, suspended electrospun polymer fibers. We present a full characterization of the culture system, including skeletal muscle sheet production and co-culturing with neuronal cell lines. The aim of the culture system is to enable the development of more realistic muscle sheets in three ways:

Firstly, the alignment of electrospun fibers encourages aligned muscle sheet formation. It has been shown that fiber-alignment augments matrix content and organization, resulting in improved mechanical properties of grown tissue [15] without slowing proliferation [16]. Aligned topographic features enhance C2C12 myotube assembly and length [17].

Secondly, suspended fibers serve as a surface for cells to attach to and grow along. As compared with typical 2D culture surfaces and even micro patterned substrates (which also encourage alignment), the suspended nature of electrospun fibers allows for more realistic growth, cell-cell interactions, morphology, and function [18, 19, 20].

Thirdly, the system incorporates a mechanism for the slow release of factors or chemicals.

Synaptogenesis is a complex process that involves more than simply the proximity of motor neurons to muscle cells, but one that must be examined within context, taking into consideration the ECM, soluble growth factors, hormones, and other small molecules that regulate formation and function [21]. We present the effect of releasing agrin, a nerve-derived protein, which has been shown to play an important role in NMJ formation, into the culture system. The system can easily be modified to allow for the slow release of other factors or proteins as well.

## **Materials and Methods**

### Electrospinning of Fibers

#### *Polymer Solutions*

Type-A porcine gelatin (Sigma-Aldrich) was used in conjunction with polycaprolactone (PCL, Sigma-Aldrich) at a ratio of 70:30, and dissolved in hexafluoro-2-propanol (HFIP, Apollo Scientific) to obtain a final concentration of 8%(w/v). PCL was chosen for its structural stability in electrospinning, and gelatin was added to increase biocompatibility. The solution was mixed inside inert Amber Vials (Supelco Analytical) to avoid glass or plastic contamination. The polymer solution was stirred at room temperature for 24h on electric rollers, visually checked for un-dissolved solute, and then used in electrospinning. Early exploratory testing (data not shown) revealed that a solute concentration of 8% results in better fiber morphology and quality as compared with the 6% solution recommended in previous studies [22, 23], which is more likely to result in beading and fibers of lower smoothness.

#### *Electrospinning Apparatus*

The electrospinning setup consists of a perspex box fed by a high pressure nitrogen supply (BOC), an exhaust tube to transfer gasses into a nearby fume hood, a syringe pump connected to the perspex box (Harvard Apparatus) via a 1/32in Polytetrafluoroethylene (PTFE) tube (Cole Parmer) through which the polymer solution is fed, and a high voltage DC source (Genvolt) generating a strong electric field between the live lead at the nozzle, from which the polymer solution is discharged, and the grounded collector plate. A secondary power supply (GW Instek) is also included for use with a rotating collector.

#### *Electrospinning Parameters*

Two collectors were used to produce different fiber arrangements. In order to electrospin randomly oriented fibers, a flat metal plate was used (Figure 1). For parallel or aligned fibers, a 5cm diameter rotating drum collector (Figure 1) was used, at 2000rpm. A nozzle distance of 15cm was used in both cases. The polymer flow rate, the high voltage source, and the Nitrogen supply were set to 0.8mL/h, 10kV, and 1 bar, respectively.

### Cell Culture and Differentiation

C2C12 (myoblastic) cells (Sigma-Aldrich) were cultured in Dulbecco's Modified Eagle Medium (DMEM, Life Technologies) supplemented with 10%(v/v) Fetal Bovine Serum (FBS, Life Technologies) and 1%(v/v) Penicillin/Streptomycin (P/S, Life Technologies). Cells were incubated at 37°C and 5% CO<sub>2</sub> in air and passaged by trypsinization every 3–4 days. Differentiation of myoblasts was achieved using two kinds of differentiation media with similar end results: 'DM1' containing 1% FBS, 1% P/S and 1% Insulin-Transferrin Selenium (ITS, Sigma-Aldrich), and 'DM2' containing 2% Horse Serum (HS, Life Technologies) and 1% P/S, both in Sodium Pyruvate-free DMEM (Sigma-Aldrich) [24].

NG108-15 (motor neuronal) cells (Sigma-Aldrich) were cultured in DMEM containing 10% FBS and 1% P/S. Passaging of NG108-15 cells was carried out by mechanical detachment, as these cells adhere lightly to the culture surface. Differentiation was induced through serum starvation and the addition of dimethyl sulfoxide (DMSO, Sigma-Aldrich) once cells were approximately 60% confluent. The differentiation medium, or 'NDM', was made up of 1.5%(v/v) DMSO, 1%(v/v) P/S and 0.5%(v/v) FBS in DMEM [25].

### Cell Staining

Staining of acetylcholine receptors (AChRs) on muscle cells was achieved with  $\alpha$ -Bungarotoxin, conjugated with AlexaFluor 594 dye (Life Technologies). Before fixing, a 1/700 dilution was added in culture media to live cells for 2h at 37°C. Cells were fixed in 3.7%(v/v) Paraformaldehyde solution (PFA, Sigma-Aldrich) in Phosphate-Buffered Saline (PBS, Fisher Scientific). For staining of intramembrane components, cells were permeabilized in PBS containing 0.1%(v/v) Tween20 (Fluka), 0.2%(v/v) Triton-X100 (Sigma-Aldrich), and 5%(w/v) Bovine Serum Albumen (BSA, Sigma-Aldrich) for 1h at 37°C and then washed three times in PBS [26]. To stain DNA and therefore identify cell

nuclei in confluent samples where individual cytoskeletons were hard to distinguish [27], a 10%(v/v) Hoechst dye (10 $\mu$ g/mL) was added (Thermo Fisher Scientific) for 30min at room temperature before fluorescent imaging. Actin filaments in both cell types were stained with Phalloidin 594 (Molecular Probes) for 1h at room temperature, and washed in PBS before imaging. For staining of  $\beta$ -III Tubulin, a neuron-specific microtubule element, rabbit anti-Tuj1 (AbCam) was used along with a goat anti-rabbit secondary antibody conjugated with AlexaFluor 488 (green) fluorescent dye (Life Technologies).

### Fiber Growth Chambers

The growth chambers described here were specifically designed to investigate the role of electrospun fibers in cell attachment, directionality, growth, and differentiation. The premise for the design was to provide a system enabling the development of cell cultures on fibers completely suspended in media, a novel outlook toward cell-fiber interactions. There are three reasons behind such rationale: (1) when there is no solid ‘secondary’ adhesion site available—contrary to the case of e.g. electrospun fibers (primary) on a coverslip (secondary)—the attachment ‘preference’ of cells to fibers can be more accurately measured; (2) fiber deterioration and breakdown can be slowed and minimized, especially important because thin and fragile fibers tend to lift off, break, or move around very easily during experimentation or transport; (3) samples can be imaged easily from inside the chambers with minimal maneuvering.

The growth chamber’s design consists of three separate silicone pieces, assembled within an imaging dish (IBIDI  $\mu$ -dish, IBIDI) and held together firmly by friction. The PDMS used was made using the Sylgard silicone elastomer kit (Dow Corning) by mixing the base and curing agent in a 10:1 ratio, followed by degasification in a vacuum chamber and subsequent injection into the desired molds. After 10min of natural degasification, the molds were cured overnight at 60°C. The bottom piece of the assembly (Figure 2A) lifts the fiber-carrying middle insert off the surface of the imaging dish. This allows for media flow around the fibers whilst keeping the samples within the working distance of conventional inverted microscopy lenses. The top piece presses down on the construct, securing fibers in place and preventing potentially disruptive movement. All pieces and systems were sterilized by ethanol immersion and under UV light for 1h prior to cell experiments.

### Cell Alignment Measurements

Hoechst-stained nuclei aspect ratios were measured by taking the ratio of the longest to the shortest dimension of the circular nuclear structure. Similarly, Phalloidin-Rhodamine stained cytoskeleton aspect ratios were measured by taking the ratio of the longest to the shortest dimension of the whole cell cytoskeleton. Cell angle standard deviations were measured using the longest cytoskeletal measurement, by computing the angle of the corresponding line from the horizontal. The standard deviations of these angles were used as a measure of cell alignment.

### Agrin Media Production and Testing

Agrin, a key protein directing clustering of acetylcholine receptors in neuromuscular development [28, 29], was investigated as a factor in co-culture. For production of agrin-containing media, Two T75 flasks with HEK293 cells (Sigma-Aldrich) at approximately 70% confluence were transfected with 36 $\mu$ g of a construct [30] expressing a soluble form of human neural agrin (donated by Dr. Judith Cossins and Prof. David Beeson) using 18 $\mu$ L polyethyleneimine and 15 $\mu$ L 20% glucose. After 24h, the medium was replaced with HEK cell growth medium. 48h later the conditioned medium was centrifuged at 2000rpm for 10min at room temperature to remove debris, aliquoted, and stored at -20°C. Agrin-containing medium was used at a 1:100 dilution in regular culture medium [30].

In culture, a slow and steady release of agrin was achieved by encapsulation in alginate. The alginate solution was prepared by mixing 1.2%(w/v) high viscosity alginic acid sodium salt from brown algae (>2000cP) (Sigma-Aldrich) in a 0.9%(w/v) solution of NaCl at 50°C on a magnetic stir plate for 30min. Pellets were then made by pipetting a solution of CaCl<sub>2</sub> onto a PDMS mold filled with the alginate solution, gelling in the desired shape. Alginate preparation was carried out under sterile conditions.

In order to approximate the release profile of agrin, this process was first carried out with an alginate solution containing fluorescein isothiocyanate-dextran (FITC-Dextran, Sigma-Aldrich) with molecular weight 70kDa, comparable in magnitude to the high molecular weight of agrin [31, 32]. Pellets containing the dye were inserted into slots created within an altered culture chamber bottom piece, as in Figure 2A. Chambers were then filled with medium, placed inside a portable incubator, and imaged for 16h at 1h intervals. The approximation of agrin release using a molecule of similar molecular weight assumes that other factors, such as the charge of the encapsulated molecule or its chemical interactions with alginate gel, do not play a determining role in its release profile [33, 34, 35].

### SEM Sample Preparation

For scanning electron microscope (SEM) imaging, cell samples were dehydrated by sequential immersion in graded ethanol (30%, 50%, 75%, 90% and 100%) for 5min per concentration, followed by critical point drying in Hexamethyldisilazane (HDMS) for 10min. Samples are then transferred onto carbon tape and attached to SEM sample holders. A Quorum SC7620 Mini Sputter Coater Glow Discharge System was used for gold-palladium coating (15s) of fiber samples, in order to enable the use of the equipment in High Vacuum mode. Fiber characterization and cell attachment images were obtained using a Carl Zeiss Evo LS15 VP-Scanning Electron Microscope.

### Methods of Analysis

Images of cells were obtained using a Nikon Inverted Fluorescent Microscope, and microscope settings were kept unchanged across related samples. Quantitative image analysis was carried out using batch-measuring tools of imaging software ImageJ/FIJI (SciJava), and results were calculated by averaging data from triplicate experiments.

### Numerical and Statistical Analysis

GraphPad Prism 6 software (La Jolla California USA) was used for data and statistical analyses. All data sets were tested for normality using the D'Agostino & Pearson omnibus normality test (the Shapiro-Wilk or Kolmogorov-Smirnov normality tests were used to supplement). For statistical analysis, tests were chosen based on normality of the data set and the number of separate versus matched samples, with p values <0.05 considered statistically significant (\* =  $p < 0.05$ , \*\* =  $p < 0.01$ , \*\*\* =  $p < 0.001$ , \*\*\*\* =  $p < 0.0001$ ). Experiments were carried out in triplicate, and data collected from three areas of each sample, from which at least three sub-areas were taken for measurements. Mean  $\pm$  standard deviation plotted for all graphs.

## **Results and Discussion**

### Fiber Characterization

In order to characterize fiber alignment and density, three different cases are examined (Figure 2B): fibers collected for 15s using the rotating collector (15s aligned), fibers collected for 30s using the rotating collector (30s aligned), and fibers collected for 30s using the standard plate collector (30s

random).

For each of the three fiber categories, three separate samples were examined and imaged, from which three image subsections were analyzed. Figure 3A summarizes the fiber alignment characterization results. The mean standard deviation of fiber angles (from the horizontal) is less than half for the rotating collector as compared with the standard plate collector. Lower angle values indicate greater alignment; therefore, fibers collected using a rotating drum collector were significantly more aligned.

Fiber density increases with collection time (Figure 3B). Additionally, the density of aligned fibers collected for a certain period of time is greater than the density of random fibers collected for the same duration. This is because the standard plate collector attracts fibers randomly across its entire surface, with a concentration gradient expanding out from the center point right underneath the nozzle, while the rotating collector concentrates fiber production onto a much smaller area.

Fiber diameter was characterized using electron microscopy of fiber samples collected directly onto carbon tape (Figure 3C). All other parameters were kept the same. Measurements in ImageJ, taken of a total of 105 fibers from nine images taken from three separate samples, yielded an average diameter of  $0.63\mu\text{m} \pm 0.13\mu\text{m}$  (Figure 3D). Electron microscopy also gave an insight into fiber morphology, showing that fibers are smooth, generally straight, and do not exhibit of beading. These observations were consistent in all samples.

Smooth, aligned fibers underpin this culture system; this structure enables enhanced matrix content and organization and results in improved mechanical properties for the scaffold. Furthermore, myotube assembly is profoundly influenced by such aligned features, resulting in enhanced myotube organization and length [15, 17].

#### FITC-Dextran Release Profile

For studies involving the slowed release of agrin or other substances into cell culture, the release profile of the alginate pellets used in our experiments as ‘substance containers’ was characterized using FITC-dextran dye. The dye was found to have a gradual and steady release into the channel and outflow area of the culture chamber. Such protracted release is sufficient to ensure continuation during cell proliferation. The release of factors in this way helps the culture system serve as a dynamic extracellular environment. Microenvironments have the potential to influence the phenotypic fate of

cells by altering gene, and ultimately protein, expression through the incorporation of growth factors and other small molecules [21].

### Cell Response to Fibers: Alignment and Morphology

To quantify muscle alignment on fibers, cells are grown using three different culture conditions: on untreated culture flasks, on aligned fibers, and on 2D uniform gelatin coatings (Figure 4D). Repeated angle measurements are taken from these samples and the mean angle standard deviations are used as a measure of alignment, a lower value indicating greater directionality. Cells grown on fibers exhibit significantly greater alignment (Figure 4A). Furthermore, cell alignment is conserved in time, during proliferation, and is transferred to uniform sheets that are formed when cell strands merge (Figure 5).

In addition to alignment analysis, analysis of cell morphology in different conditions can yield interesting insights into cell mechanisms employed during fiber attachment. Cytoskeleton morphology and nucleus morphology were both studied qualitatively and quantitatively.

Qualitative inspection indicates the existence of three predominant cell profiles in early attachment phases. These are referred to as *spindle*, *parallel*—as designated in relevant literature [36]—and, introduced here, *cross*. Figure 6 (left) depicts physical characteristics, typical force interactions with fibers, as well as real occurrences of these shapes in samples. Visual inspection of various samples identifies *parallel* and *spindle* shapes as the most commonly occurring. *Cross* shapes are less prevalent, potentially due to the rare occurrence of precisely perpendicular fibers.

The three attachment profiles are subject to varied fiber interactions, which in turn affect cell proliferation behavior. In *parallel* and *cross* cases, cell cytoskeletons span the spaces between fibers, resulting in a tensile force as cells grow and spread. This force acts on the fibers in a direction perpendicular to their orientation, and it can explain the holes observed in long-term sheet cultures (Figure 5 and Figure 7).

Nuclei and cytoskeletons of cells in these samples were stained, as seen in Figure 6, with Phalloidin (for actin, red) and Hoechst (for DNA, blue), in order to measure nucleus and cytoskeleton aspect ratios. Figure 4B-C displays the result of 500 aspect ratio measurements, nucleus and cytoskeleton respectively, taken from four different samples of each condition.

Cells grown on fibers exhibit a significantly higher degree of nucleus stretching or deformation,

compared to those grown on a flat surface, whether culture flask or uniform gelatin layer (Figure 4B). These findings are increasingly apparent in cytoskeletal aspect ratio analysis. Unlike the nucleus of a cell, which can only exhibit a very limited amount of deformation, the cytoskeleton can stretch more easily along fibers. Figure 4C indicates that cytoskeletal aspect ratios for cells grown on fibers can on average be greater than double that of cells grown on flasks. These findings are in line with previous studies indicating that C2C12 cells exhibit greater cytoskeletal length on aligned topographies, in turn enabling the growth of longer myotubes upon differentiation [17].

### Cell Spread and Differentiation on Fibers

#### *C2C12 Cell Spreading*

Fiber morphology has a notable effect on cell growth. In the case of aligned fibers, initial cell growth is typically parallel to the fiber direction, attaching all along the lengths of the fibers before spreading outward laterally—eventually forming a uniform cell sheet. Figure 5 tracks the phases of cell proliferation, beginning with attachment and ending with the formation of a uniform muscle sheet. Higher fiber density results in faster sheet formation, the rate of which can be characterized by measuring the average size of ‘holes’ in the growing muscle layer. Conversely, in the case of randomly aligned fibers, complete muscle sheets do not typically form. Cells spread along fibers, and then tend to cluster at the fiber junction points. While these clusters increase in thickness, their growth is typically limited, and never sufficient to coalesce into a complete monolayer. The free spaces that exist between fibers, for samples with an initial seeding density of  $\approx 1$  million cells/mL and  $\approx 1.5$  million cells/mL, are characterized in Figure 7i and Figure 7ii respectively. A decrease in cell-free area indicates muscle sheet development. It is also evident that increased seeding density decreases the amount of time required for the formation of a complete monolayer on both 15s and 30s fibers ( $p < 0.0001$  for 15s aligned fibers and  $p < 0.005$  for 30s aligned fibers, 2way ANOVA + Sidak’s MCT). The process occurs faster on 30s fibers, confirming that fiber density and seeding density both serve a crucial role in determining the rate of sheet formation. Fiber density plays an additional role in the number of holes that form during the process; denser fibers result in smaller intra-fiber spaces, and thus a decreased likelihood of hole formation.

Cells that attach to parallel fibers tend to grow in similar directions, spreading laterally after the fibers

are covered and only when there are 'bridgeable' gaps that can be scaled directionally. The general shape/direction of the fibers is retained. Cells that attach to random fibers do not grow in a common direction, as each cell proliferates along its own 'host' fiber. The cytoskeletons of the cells produce opposing forces on the fibers, leaving larger gaps between muscle strands and clusters. Figure 7iii provides an analysis of strand thickness in time (for random fibers), indicating that cells aggregate onto strands of growing thickness up until a certain point, after which the strand thickness begins to decrease. This could be due to cells dying off or cells reaching a weight threshold per supporting fiber.

### *C2C12 Cell Differentiation on Fibers*

As discussed previously, C2C12 myoblast differentiation can be induced through changes in culture media. Myotubes begin to form a few days after exposure to this differentiation media, initially appearing as multinucleated, protracted bodies embedded within the myoblast layer (only bodies with greater than eight nuclei were counted as myotubes for the purpose of the following analyses). In the experiments presented here, differentiation is induced on fibers following the successful formation of a uniform muscle layer in proliferation media after 72h (Figure 7A-L). Figure 8B summarizes the obtained results, highlighting the fact that fibers may affect the length of the differentiating myotubes, as observed through morphological observations. Figure 8A reveals a significantly lower angle standard deviation for myotubes growing on fibers as compared with that of myotubes growing on flasks, which indicates that the initial fiber orientation is retained throughout the differentiation process. This is advantageous due to the overall goal of maintaining alignment for longer myotube formation [17].

### Co-Culture and Agrin Experiment Results

In co-culture experiments, C2C12 cells were seeded at high density (>1.5 million cells/mL) on 30s aligned fibers and cultured for 72h on proliferation media. NG108-15 cells were added onto the resulting muscle sheet after 72h (>1 million cells/mL), and were left to grow for at least 48h in proliferation media.  $\beta$ -III Tubulin (Tuj1) staining revealed aligned neurites extending in the direction of the underlying fibers, indicating a level of interaction between fiber alignment and neurons seeded onto C2C12 sheets. Two likely explanations for this observation are that (1) neurites extend *through* the muscle sheet, using the fibers themselves for guidance, or (2) neurites extend between C2C12

cytoskeletons, which are independently aligned with the fibers.

Figure 8C suggests that standard deviations of neurite angles are significantly lower for co-cultures on fibers, as compared with those for co-cultures on 2D flasks. In other words, neurite alignment is higher for neurons in fiber co-cultures, implying that these methods can be utilized for custom development of aligned innervated muscle sheets. Figure 9C-D depicts co-cultures on an untreated flask and on fibers respectively.

To quantify the effect of agrin, which is a nerve-derived protein, on AChR clustering within these samples, 50% of fiber co-cultures were incubated with agrin-containing alginate pellets that slowly delivered agrin to the system over 48h. Agrin is known to promote AChR clustering during synaptogenesis through activation of muscle-specific kinase [37].  $\alpha$ -Bungarotoxin staining revealed the expression of AChRs on muscle cells, with summarized results in Figure 9A-B, and images in Figure 9E-F. The quantifications suggest that total area coverage of AChRs (red-stained tissue) is significantly greater in samples supplemented with agrin-containing pellets, confirming that muscle sheets grown in this system are capable of forming AChR clusters in response to agrin [37]. On the other hand, based on this study, there is no conclusive evidence of agrin's role on the clustering *density* of receptors, i.e. cluster brightness, in a given location.

These results indicate that the system can be used to deliver certain proteins and other relevant factors to the cell culture, enabling the creation of biomimetic approaches to *in vitro* muscle sheet, and henceforth NMJ, development.

## Conclusions

Tissue engineering approaches have rendered *in vitro* muscle growth a feasible option for biological research; however, current technologies are not yet capable of adequately mimicking *in vivo* tissue [38]. Reproducing natural muscle architecture is an important step in muscle engineering, given that skeletal muscle is comprised of fibrils whose structural arrangement determines functionality. For this reason, the alignment of myoblasts is a pivotal preparatory step for the development of myotubes during musculoskeletal myogenesis. The capacity to quickly and successfully align myoblasts for myotube formation *in vitro* would serve as a great benefit to the field of tissue engineering [38].

Furthermore, recent studies have revealed abnormal behavior in cells extracted from their natural 3D environments and transferred to 2D monolayers. This highlights the necessity for the reproduction of essential matrix factors if biologically valid conclusions are to be collected from *in vitro* cell culture and experimentation [21].

As summarized in this paper, *in vitro* studies of NMJs grown in co-culture chambers have served as a proof of concept that electrospun fibers can be used in simple recreations of suspended co-culture, allowing for desired alignment, maturation of cells, and gradual release of relevant factors. Myoblast angle standard deviations were found to be lower on fibers than on untreated culture flasks by a factor of 5. Myoblast nucleus aspect ratios increased by 20% on fibers, and cytoskeleton stretching increased from an average of 1.8 ( $\pm 0.2$ ) on flasks to 5 ( $\pm 2$ ) on fibers. By seeding NG108-15 cells onto fully developed C2C12 monolayers, it was shown that neurites extend parallel to underlying fibers, which help guide innervation patterns. The standard deviation of neurite extension angles was found to be lower on fiber-grown co-cultures compared to those grown on untreated flasks (by a factor of 3). This result demonstrates that the culture system can be successfully used to influence directionality of innervation in artificial muscle sheets. Furthermore, fluorescent imaging of co-cultures containing agrin media showed significant increase in AChR occurrence (approximately 50%).

Further investigation into mechanisms influencing the development of cell sheets on suspended fibers could lead to a better understanding of cell behavior, allowing for more precise manipulation of culture outcomes in preparation for future NMJ development. Studies to better understand the muscle innervation and NMJ maturation process must also be extended through functionality tests. This will help to elucidate the interplay of aligned suspended matrices, bio-artificial muscle sheets, innervation, and intercellular interactions during maturation and functional response. This, coupled with broader testing of agrin and other relevant factors, could lead to the development of a robust model for *in vitro* study of the physiological processes underlying ageing and pathological neuromuscular degeneration. Such comprehensive models would facilitate the development of innovative approaches to the prevention and treatment of neurological conditions.

## Acknowledgements

This research was supported by the China Regenerative Medicine International (CRMI), the Biotechnology and Biological Sciences Research Council (BBSRC), the Engineering and Physical Sciences Research Council (EPSRC), and the Clarendon Fund through Oxford University Press (OUP). Many thanks to Dr. Judith Cossins and Prof David Beeson for donating the agrin construct used in experiments. The support of the Laboratory for In-situ Microscopy and Analysis (LIMA) and that of Christ Church is also gratefully acknowledged.

## References

- [1] Wu H, Xiong WC, Mei L. To build a synapse: signaling pathways in neuromuscular junction assembly. *Development*. 2010;137(7):1017–1033.
- [2] Fischer L, Culver D, Tennant P, Davis A, Wang M, Castellano-Sanchez A, et al. Amyotrophic lateral sclerosis is a distal axonopathy: evidence in mice and man. *Exp Neurol*. 2004 February;185(2):232–40.
- [3] Spaulding E, Sleigh JN, Morelli K, Pinter M, Burgess R, Seburn K. Synaptic Deficits at Neuromuscular Junctions in Two Mouse Models of Charcot-Marie-Tooth Type 2d. *J Neurosci*. 2016 March;36(11):3254–67.
- [4] Murray L, Comley L, Thomson D, Parkinson N, Talbot K, Gillingwater TH. Selective vulnerability of motor neurons and dissociation of pre- and post-synaptic pathology at the neuromuscular junction in mouse models of spinal muscular atrophy. *Human Molecular Genetics*. 2008 April;17(7):949–62.
- [5] Alonso A, Logroscino G, Jick SS, Hernan MA. Incidence and lifetime risk of motor neuron disease in the United Kingdom: a populationbased study. *European journal of neurology*. 2009;16(6):745–751.
- [6] Olesen J, Gustavsson A, Svensson M, Wittchen H, Jönsson B. The economic cost of brain disorders in Europe. 2012 January;19(1):155–62.
- [7] Talbot K. Motor Neurone Disease. *Postgraduate medical journal*. 2002 July;78(923):513–519.
- [8] Southam KA, King A, Blizzard C, McCormack G, Dickson T. Microfluidic primary culture model of the lower motor neuron-neuromuscular junction circuit. *Journal of Neuroscience Methods*.

2013 September;218(2):164–169.

- [9] Mars T, Yu K, Tang X, Miranda A, Grubic Z, Cambi F, et al. Differentiation of glial cells and motor neurons during the formation of neuromuscular junctions in cocultures of rat spinal cord explant and human muscle. *Journal of Comparative Neurology*. 2001;438(2):239–251.
- [10] Baker BM, Chen CS. Deconstructing the third dimension – how 3D culture microenvironments alter cellular cues. *Journal of Cell Science*. 2012;125(13):3015–3024.
- [11] Bourget JM, Guillemette M, Veres T, Auger FA, Germain L. Alignment of cells and extracellular matrix within tissue-engineered substitutes. INTECH Open Access Publisher; 2013.
- [12] Huang N, Lee R, Li S. Engineering of aligned skeletal muscle by micropatterning. *Am J Transl Res*. 2010;2(1):43–55.
- [13] Ostrovidov S, Hosseini V, Ahadian S, Fujie T, Parthiban S, Ramalingam M, et al. Skeletal muscle tissue engineering: methods to form skeletal myotubes and their applications. *Tissue Engineering Part B: Reviews*. 2014;20(5):403–436.
- [14] Cheema U, Yang S, Mudera V, Goldspink G, Brown R. 3D in vitro model of early skeletal muscle development. *Cell motility and the cytoskeleton*. 2003;54(3):226–236.
- [15] Baker BM, Mauck RL. The effect of nanofiber alignment on the maturation of engineered meniscus constructs. *Biomaterials*. 2007;28(11):1967–1977.
- [16] Venugopal JR, Ma L, Yong T, Ramakrishna S. In vitro study of smooth muscle cells on polycaprolactone and collagen nanofibrous matrices. *Cell Biology International*. 2005;29(10):861–867.
- [17] Lanfer B, Seiba FP, Freudenberg U, Stamov D, Bley T, Bornh user M, et al. The growth and differentiation of mesenchymal stem and progenitor cells cultured on aligned collagen matrices. *Biomaterials*. 2009;30(30):5950–5958.
- [18] Haga JH, Li YSJ, Chien S. Molecular basis of the effects of mechanical stretch on vascular smooth muscle cells. *Biomaterials*. 2007;40(5):947–960.
- [19] Yim EK, Reano RM, Pang SW, Yee AF, Chen CS, Leong KW. Nanopattern-induced changes in morphology and motility of smooth muscle cells. *Biomaterials*. 2005;26(26):5405–5413.
- [20] Soliman E, Yang SC, Dombi GW, Bhatia SK. Electrically conductive, biocompatible composite containing carbon nanobrushes for applications in neuroregeneration. *IEEE Northeast Bioengineering*

Conference 2012. 2012 March;38:16–18.

- [21] Tibbitt MW, Anseth KS. Hydrogels as extracellular matrix mimics for 3D cell culture. *Biotechnology and Bioengineering*. 2009;103(4):655–663.
- [22] Liu Y, He JH, Yu Jy, Zeng Hm. Controlling numbers and sizes of beads in electrospun nanofibers. *Polymer International*. 2008;57(4):632–636.
- [23] Huang ZM, Zhang Y, Kotaki M, Ramakrishna S. A review on polymer nanofibers by electrospinning and their applications in nanocomposites. *Composites science and Technology*. 2003 April;63:2223–2253.
- [24] Fisher-Aylor K, Williams B. Cell Growth Protocol and Differentiation Treatment for the C2C12 Cell Line; 2011. <https://genome.ucsc.edu/>.
- [25] Schubert D, Humphreys S, De Vitry F, Jacob F. Induced Differentiation of a Neuroblastoma. *Developmental Biology*. 1971;25:514–546.
- [26] Jamur MC, Oliver C. Permeabilization of Cell Membranes. *Immunocytochemical Methods and Protocols, Methods in Molecular Biology*. 2010;588:63–66.
- [27] Latt S, Stetten G, Juergens L, Willard H, Scher C. Recent developments in the detection of deoxyribonucleic acid synthesis by 33258 Hoechst fluorescence. *J Histochem Cytochem*. 1975 July;23(7):493–505.
- [28] Nitkin R, Smith M, Magill C, Fallon J, Yao Y, Wallace B, et al. Identification of agrin, a synaptic organizing protein from Torpedo electric organ. *J Cell Biol*. 1987 Dec;105(6 Pt 1):2471–8.
- [29] Ferns M, Campanelli J, Hoch W, Scheller R, Hall ZW. The ability of agrin to cluster AChRs depends on alternative splicing and on cell surface proteoglycans. *Neuron*. 1993 September;11(3):491–502.
- [30] Koneczny I, Cossins J, Waters P, Beeson D, Vincent A. MuSK Myasthenia Gravis IgG4 Disrupts the Interaction of LRP4 with MuSK but Both IgG4 and IgG1-3 Can Disperse Preformed Agrin-Independent AChR Clusters. *Plos One*. 2013 Nov;8(11).
- [31] Bowe M, Fallon J. The Role of Agrin in Synapse Formation. *Annual Review of Neuroscience*. 1995;18:443–462.
- [32] Hoch W, Campanelli JT, Scheller RH. Agrin-induced clustering of acetylcholine receptors: a

cytoskeletal link. *J Cell Biol.* 1994 July;126(1):1–4.

[33] Kim CK, Lee EJ. The controlled release of blue dextran from alginate beads. *International Journal of Pharmaceutics.* 1992 February;79(1–3):11–19.

[34] Gombotz WR, Wee SF. Protein release from alginate matrices. *Advanced Drug Delivery Reviews.* 2012 December;64:194–205.

[35] Kikuchi A, Kawabuchi M, Sugihara M, Sakurai Y, Okano T. Pulsed dextran release from calcium-alginate gel beads. *Journal of Controlled Release.* 1997 July;47(1):21–29.

[36] Sheets K, Wang J, Meehan S, Sharma P, Ng C, Khan M, et al. Cell-Fiber Interactions on Aligned and Suspended Nanofiber Scaffolds. *Journal of Biomaterials and Tissue Engineering.* 2013;3(4):355–368.

[37] Wang, L., Shansky, J. & Vandenberg, H. Induced Formation and Maturation of Acetylcholine Receptor Clusters in a Defined 3D Bio-Artificial Muscle. *Mol Neurobiol.* 2013; 48: 397.

[38] Lam MT, Sim S, Zhu X, Takayama S. The effect of continuous wavy micropatterns on silicone substrates on the alignment of skeletal muscle myoblasts and myotubes. *Biomaterials.* 2006;27(24):4340–4347.

### List of Figure Legends:

**Figure 1:** Electrospinning nozzle diagram (top left) and image (top right) with a standard flat-plate metal collector (as would be used for random fiber collection). Bottom: Rotating drum collector used for spinning aligned fibers.

**Figure 2:** (A) Culture chamber components: top piece used to clamp fibers in place and keep system stable, 30mm wide and 3mm thick; middle piece used for fiber suspension, 15mm and 1mm; and bottom 'prop' piece, 20mm and 1mm. Scale bar = 1cm. (B) Fiber samples: fibers collected for 15s on rotating drum collector (15s aligned), fibers collected for 30s on rotating drum collector (30s aligned), fibers collected for 30s on flat-plate collector (30s random). Scale bar = 100 $\mu$ m.

**Figure 3:** (A) Standard deviation of 'angle from horizontal' measurements for different collection parameters. Lower values indicate greater alignment. 3 samples, >80 measurements per sample. (B) Fiber density per millimeter. 9 samples per category. One-way ANOVA + Turkey's MCT. (C) ESEM fiber diameter characterization, High Vacuum mode, 10,000x magnification. Scale bars = 5 $\mu$ m. (D) Histogram of fiber diameters.

**Figure 4:** (A) Angle standard deviations of 48h C2C12 cultures. (B) C2C12 nuclei aspect ratios (a value of 1 indicates a round object, and values >1 indicate an elongated object). (C) C2C12 cytoskeletal aspect ratios. (D) Cell alignment samples: C2C12 cells (left) on untreated flask, (middle) on aligned fibers, and (right) on a uniform gelatin layer. Scale bar = 100 $\mu$ m. A: One-Way ANOVA + Turkey's MCT. B-C: Kruskal-Wallis + Dunn's MCT. (>200 samples per condition).

**Figure 5:** C2C12 spreading on 15s aligned fibers, showing retained alignment following the merging of cell strands into a uniform layer. Scale bar = 100 $\mu$ m.

**Figure 6:** (Left, top) Cell shape classifications with diagrams of forces exerted by cell cytoskeleton on fibers; (Left, middle) Samples from each classification; (Left, bottom) Samples stained for actin (red,

Phalloidin) and DNA (blue, Hoechst) on suspended fibers. White arrows mark fibers and yellow arrows indicate intended fiber alignment direction. Scale bars =  $50\mu\text{m}$ . **(A)** Extreme case of elongated spindle cells showing nucleus deformation and thinly stretched cytoskeleton; **(B)** cross cell which has adhered at the intersection of several fibers and exhibits cytoskeletal deformation; **(C)** parallel cell with circular nucleus but cytoskeletal deformation in both parallel and tangential directions to fibers; **(D)** cells on untreated control flask with circular nucleus and cytoskeleton. Actin (red, Phalloidin) and DNA (blue, Hoechst) staining. Scale bars =  $50\mu\text{m}$ .

**Figure 7:** Plots of intra-fiber free space from 24h to 120h in culture proliferation media. Initial seeding density of **(i)**  $1 \times 10^6$  cells/mL and **(ii)**  $1.5 \times 10^6$  cells/mL. **(iii)** An analysis of C2C12 growth by looking at strand thickness on randomly aligned fibers. i-ii: 2way ANOVA + Turkey's MCT. iii: Kruskal-Wallis + Dunn's MCT. **(A-D)** Cell spreading on 15s aligned fibers, **(E-H)** 30s aligned fibers, and **(I-L)** random fibers, after 24h (first column), 48h (second column), 72h (third column), and 120h (fourth column). Scale bar =  $100\mu\text{m}$ .

**Figure 8:** **(A)** Myotube angle standard deviation and **(B)** myotube length for C2C12 cells after 216h (168h on ITS-supplemented differentiation media) on untreated culture flasks and 30s aligned fibers. 2 samples per category, >40 measurements per sample. **(C)** NG108-15 neurite angle standard deviations in co-cultures with C2C12s, on flasks and fibers. A-C: Unpaired t-test.

**Figure 9:** Acetylcholine receptor presence in terms of **(A)** area coverage and **(B)** density by cluster brightness in co-cultures with and without agrin. One way ANOVA + Dunnett's and Sidak's MCT. Neurite extension in co-cultures on **(C)** untreated flask and **(D)** on fibers. Co-cultures on fibers **(E)** without and **(F)** with agrin. **(G)** C2C12 myotube and NG108-15 co-culture, with arrows indicating junction sites. Images show neuronal  $\beta$ -III Tubulin (green, Tuj1) and AChR (red,  $\alpha$ -Bungarotoxin) staining. Scale bars =  $100\mu\text{m}$ .

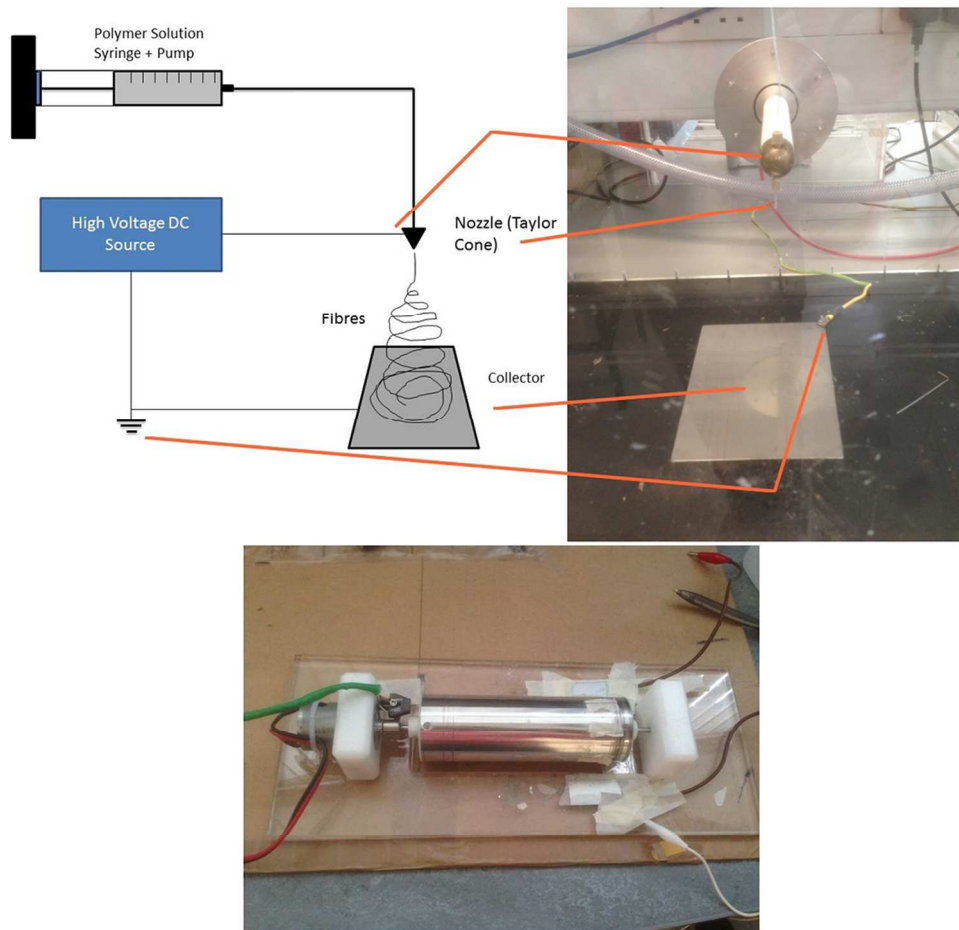


Figure 1: Electrospinning nozzle diagram (top left) and image (top right) with a standard flat-plate metal collector (as would be used for random fiber collection). Bottom: Rotating drum collector used for spinning aligned fibers.

101x94mm (300 x 300 DPI)

ACCE

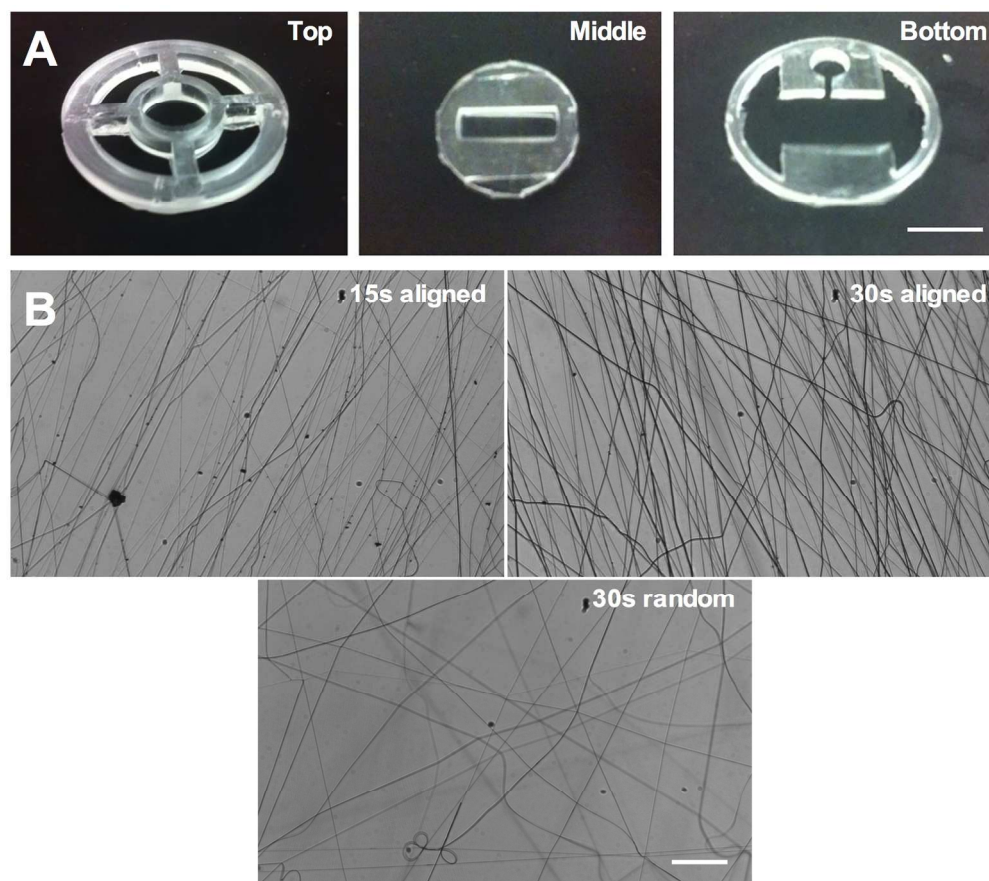


Figure 2: (A) Culture chamber components: top piece used to clamp fibers in place and keep system stable, 30mm wide and 3mm thick; middle piece used for fiber suspension, 15mm and 1mm; and bottom 'prop' piece, 20mm and 1mm. Scale bar = 1cm. (B) Fiber samples: fibers collected for 15s on rotating drum collector (15s aligned), fibers collected for 30s on rotating drum collector (30s aligned), fibers collected for 30s on flat-plate collector (30s random). Scale bar = 100 $\mu$ m.

162x143mm (300 x 300 DPI)

Accf

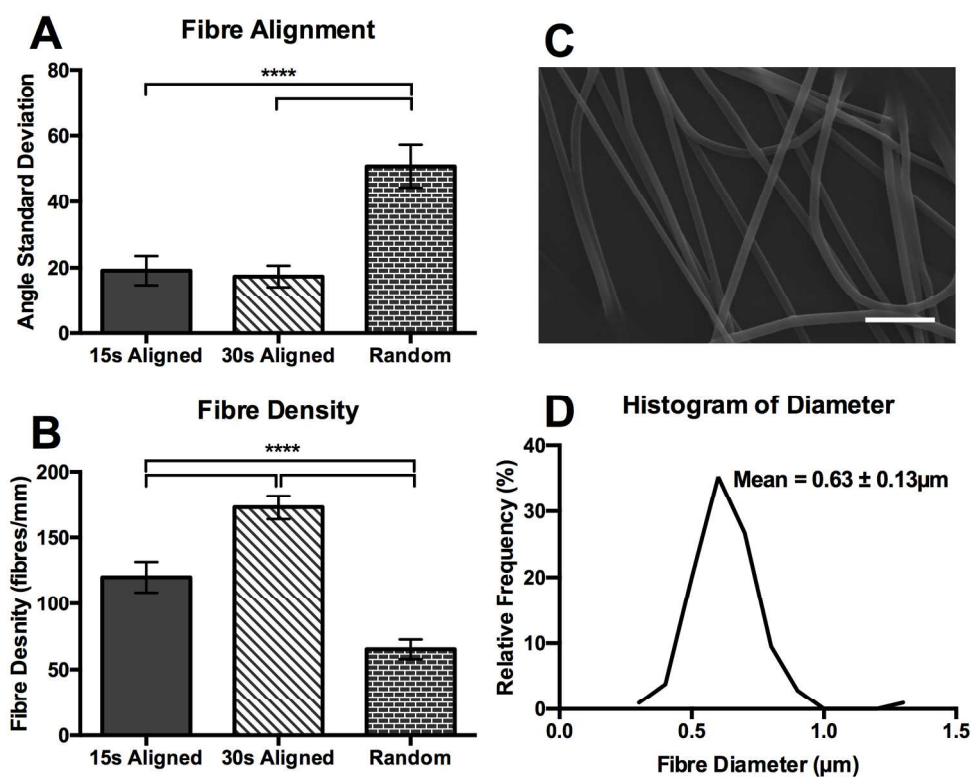


Figure 3: (A) Standard deviation of 'angle from horizontal' measurements for different collection parameters. Lower values indicate greater alignment. 3 samples, >80 measurements per sample. (B) Fiber density per millimeter. 9 samples per category. One-way ANOVA + Turkey's MCT. (C) ESEM fiber diameter characterization, High Vacuum mode, 10,000x magnification. Scale bars =  $5 \mu\text{m}$ . (D) Histogram of fiber diameters.

173x139mm (300 x 300 DPI)

Acce] ]

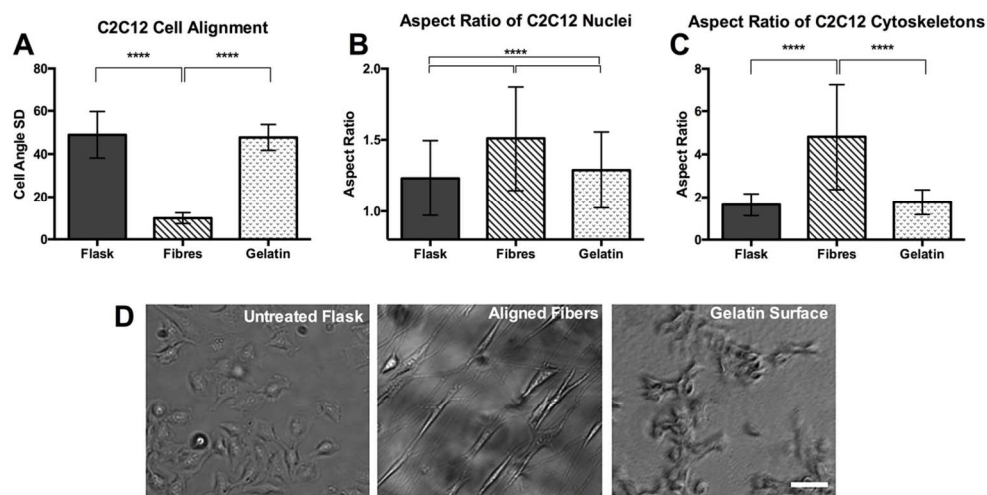


Figure 4: (A) Angle standard deviations of 48h C2C12 cultures. (B) C2C12 nuclei aspect ratios (a value of 1 indicates a round object, and values >1 indicate an elongated object). (C) C2C12 cytoskeletal aspect ratios. (D) Cell alignment samples: C2C12 cells (left) on untreated flask, (middle) on aligned fibers, and (right) on a uniform gelatin layer. Scale bar = 100 $\mu$ m. A: One-Way ANOVA + Turkey's MCT. B-C: Kruskal-Wallis + Dunn's MCT. (>200 samples per condition).

110x56mm (300 x 300 DPI)

Accepte

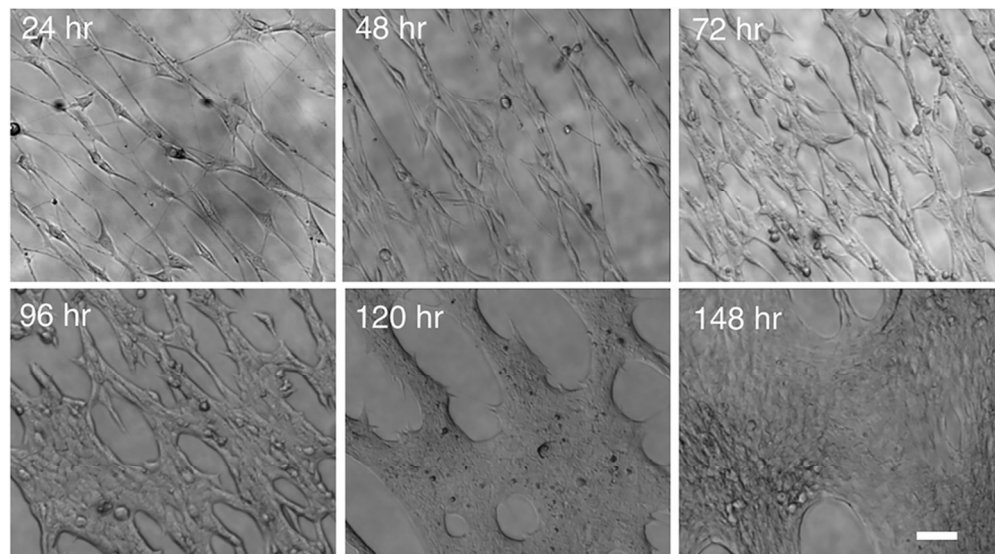


Figure 5: C2C12 spreading on 15s aligned fibers, showing retained alignment following the merging of cell strands into a uniform layer. Scale bar = 100 $\mu$ m.

83x46mm (300 x 300 DPI)

Accepted

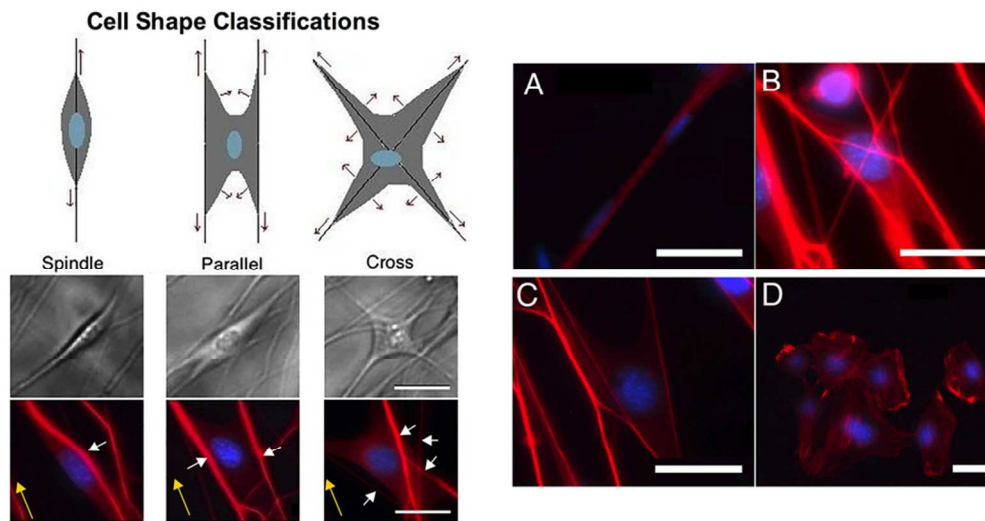


Figure 6: (Left, top) Cell shape classifications with diagrams of forces exerted by cell cytoskeleton on fibers; (Left, middle) Samples from each classification; (Left, bottom) Samples stained for actin (red, Phalloidin) and DNA (blue, Hoechst) on suspended fibers. White arrows mark fibers and yellow arrows indicate intended fiber alignment direction. Scale bars = 50µm. (A) Extreme case of elongated spindle cells showing nucleus deformation and thinly stretched cytoskeleton; (B) cross cell which has adhered at the intersection of several fibers and exhibits cytoskeletal deformation; (C) parallel cell with circular nucleus but cytoskeletal deformation in both parallel and tangential directions to fibers; (D) cells on untreated control flask with circular nucleus and cytoskeleton. Actin (red, Phalloidin) and DNA (blue, Hoechst) staining. Scale bars = 50µm.

82x44mm (300 x 300 DPI)

Accepted

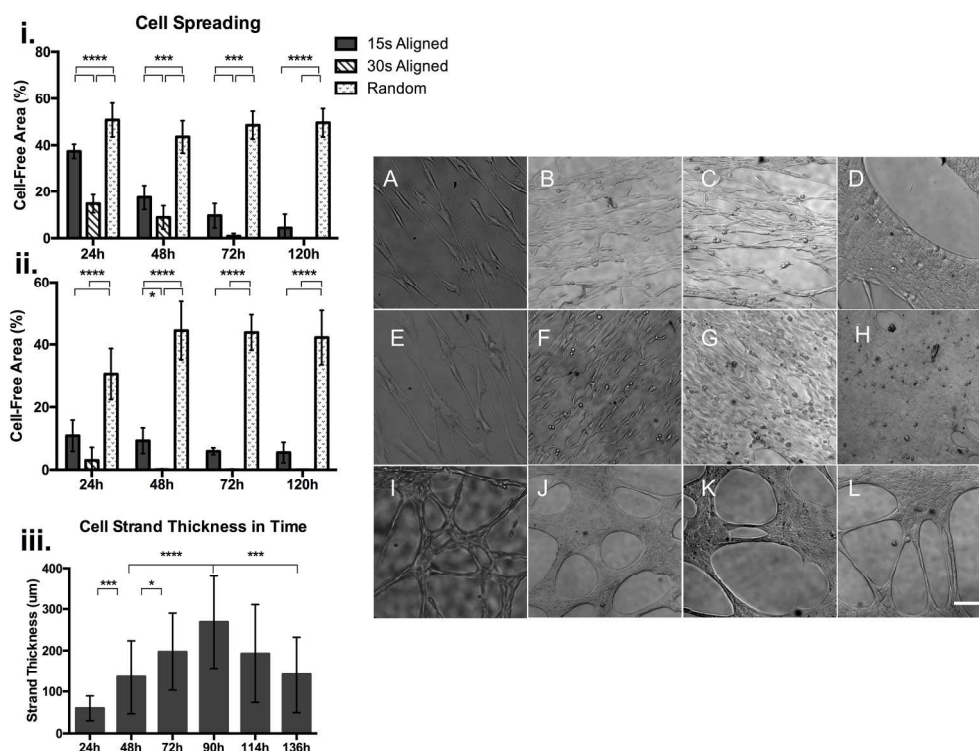


Figure 7: Plots of intra-fiber free space from 24h to 120h in culture proliferation media. Initial seeding density of (i)  $1 \times 10^6$  cells/mL and (ii)  $1.5 \times 10^6$  cells/mL. (iii) An analysis of C2C12 growth by looking at strand thickness on randomly aligned fibers. i-ii: 2way ANOVA + Turkey's MCT. iii: Kruskal-Wallis + Dunn's MCT. (A-D) Cell spreading on 15s aligned fibers, (E-H) 30s aligned fibers, and (I-L) random fibers, after 24h (first column), 48h (second column), 72h (third column), and 120h (fourth column). Scale bar =  $100 \mu\text{m}$ .

192x148mm (300 x 300 DPI)

Accel

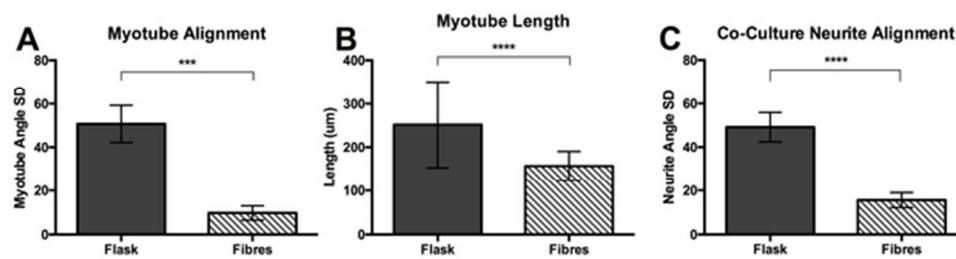


Figure 8: (A) Myotube angle standard deviation and (B) myotube length for C2C12 cells after 216h (168h on ITS-supplemented differentiation media) on untreated culture flasks and 30s aligned fibers. 2 samples per category, >40 measurements per sample. (C) NG108-15 neurite angle standard deviations in co-cultures with C2C12s, on flasks and fibers. A-C: Unpaired t-test.

55x15mm (300 x 300 DPI)

Accepted A

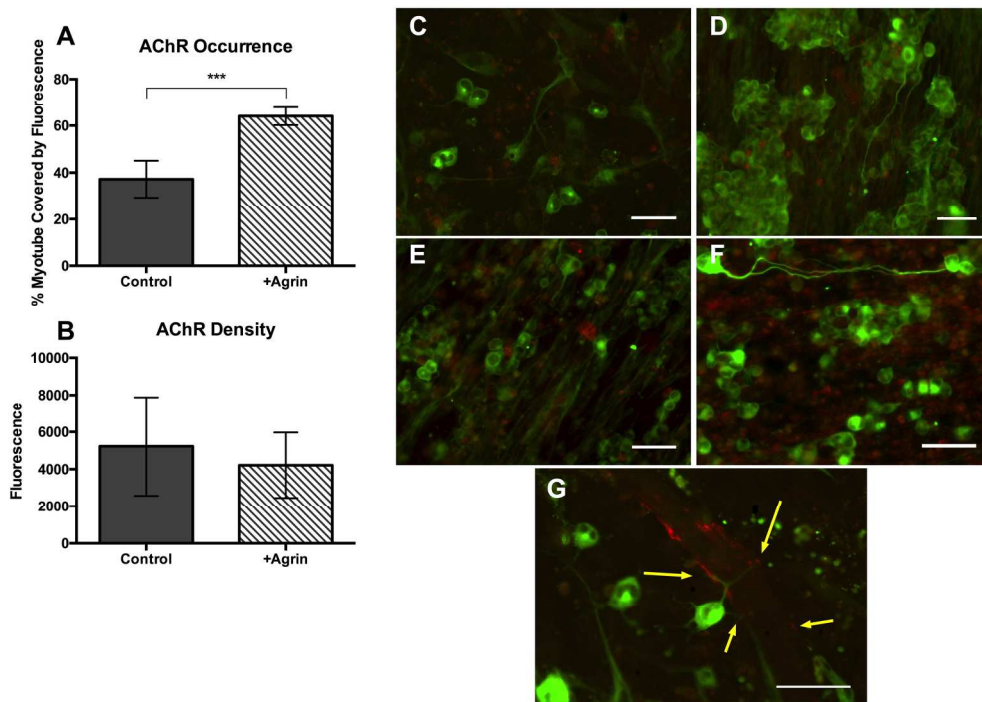


Figure 9: Acetylcholine receptor presence in terms of (A) area coverage and (B) density by cluster brightness in co-cultures with and without agrin. One way ANOVA + Dunnett's and Sidak's MCT. Neurite extension in co-cultures on (C) untreated flask and (D) on fibers. Co-cultures on fibers (E) without and (F) with agrin. (G) C2C12 myotube and NG108-15 co-culture, with arrows indicating junction sites. Images show neuronal  $\beta$ -III Tubulin (green, Tuj1) and AChR (red,  $\alpha$ -Bungarotoxin) staining. Scale bars = 100 $\mu$ m.

191x134mm (300 x 300 DPI)

Accep